Directional difference of the spin angular-momentum density and spin vectors in tightly focused bichromatic optical Lissajous beams

Xinlu Zhu,[1] Xiangyun Li,[1] Zhen Dong,[1,2] Fei Wang,[1] Lin Liu,[1] Andreas Norrman [●],[2] Tero Setälä,[2,3,*]
Yangjian Cai,[3,4,†] and Yahong Chen [●][1,‡]

[1]*School of Physical Science and Technology, Soochow University, Suzhou 215006, China*
[2]*Center for Photonics Sciences, University of Eastern Finland, P.O. Box 111, 80101 Joensuu, Finland*
[3]*Shandong Provincial Engineering and Technical Center of Light Manipulation and Shandong Provincial Key Laboratory of Optics and
Photonic Devices, School of Physics and Electronics, Shandong Normal University, Jinan 250014, China*
[4]*Joint Research Center of Light Manipulation Science and Photonic Integrated Chip of East China Normal University and
Shandong Normal University, East China Normal University, Shanghai 200241, China*

The spin angular-momentum density vector and the so-called spin vector reflecting the polarization properties of a light field are parallel for a monochromatic light field whose polarization ellipse at a point necessarily lies in a fixed plane. In contrast, the electric field of polychromatic light may, in general, evolve in three directions such that the average intensity in all of them is nonzero for any orientation of the reference frame. Consequently, the two vectors are no longer necessarily parallel. In this work we consider tightly focused bichromatic Lissajous beams and show that the spin angular-momentum density vector and the spin vector in such three-dimensional light fields may point in markedly different directions, almost orthogonal in some cases, and thus generally provide different information on the spin of light.

I. INTRODUCTION

The spin angular momentum (SAM) is a fundamental property in electrodynamics [1–8], while the so-called spin vector, describing the helicity and direction around which the electric field circulates, is an important polarimetric quantity [9–11]. The local SAM is quantified by the SAM density vector, which in the case of monochromatic light field is parallel to the spin vector. Hence, for a monochromatic field the two vectors provide the same directional information on the spin and are practically interchangeable [12]. The assumption of monochromaticity is often adequate and it has been applied, e.g., to studies concerning the transverse nature of spin in evanescent waves [4,5,13] and focal fields [4,5,14–16].

For polychromatic fields, however, the connection between the directions of the SAM density vector and spin vector is more elusive. In the case of polychromatic two-dimensional (2D) fields (beams and far fields), the electric vector is restricted to a plane and the two vectors are either parallel or antiparallel, depending on the spectral helicity properties [12]. Even more freedom with the directions is found for genuine 3D fields whose characteristic property is that the intensities of the Cartesian field components are nonzero for any orientation of the frame. Such fields are common in nano optics and other situations involving highly nonparaxial light [17,18]. The general formalism for the possible distinct directions of the SAM density and spin vectors in the case of polychromatic 3D light was given in [12], but no explicit physical situation where the effect occurs has been explored. In this work we consider tight focusing of bichromatic Lissajous beams and demonstrate that in the focal plane the two vectors can be almost orthogonal. Therefore, the complementary information the two vectors carry about the spin of light can be highly different.

This paper is structured as follows. In Sec. II we consider superpositions of monochromatic optical fields and derive expressions for the related (electric) SAM density vector and spin vector. We further introduce the polarization descriptors needed in this work. The Lissajous beams are introduced in Sec. III and the spin properties of the focal fields they generate are studied in Sec. IV. In Sec. V we summarize the main conclusions.

II. SUPERPOSITION OF MONOCHROMATIC ELECTRIC FIELDS

A. SAM density and spin vectors

Consider an electric field composed of N monochromatic components of different frequencies. At an instant of time t it can be written as $\mathbf{E}(t) = \mathrm{Re}[\boldsymbol{\mathcal{E}}(t)]$, where Re denotes the real part and

$$\boldsymbol{\mathcal{E}}(t) = \sum_{n=1}^{N} \mathbf{E}_n e^{-i\omega_n t}, \tag{1}$$

with $\mathbf{E}_n$ the three-component (complex, column) Jones vector that represents the local polarization state at (positive) angular

*tero.setala@uef.fi
†yangjian_cai@163.com
‡yahongchen@suda.edu.cn

frequency ω_n. The dual-symmetric form of the electric SAM density vector is [1,3,7,8]

$$\mathbf{S}(t) = \frac{\epsilon_0}{2}\mathbf{E}(t) \times \mathbf{A}(t), \tag{2}$$

where ϵ_0 is the vacuum permittivity and $\mathbf{A}(t)$ is the real-value vector potential that satisfies $\mathbf{E}(t) = -d\mathbf{A}(t)/dt$. In analogy to the electric field, the vector potential can be written as $\mathbf{A}(t) = \text{Re}[\boldsymbol{\mathcal{A}}(t)]$, where $\boldsymbol{\mathcal{A}}(t) = \sum_{n=1}^{N} \mathbf{A}_n e^{-i\omega_n t}$, with the amplitudes obeying $\mathbf{E}_n = i\omega_n \mathbf{A}_n$.

Inserting $\mathbf{E}(t)$ and $\mathbf{A}(t)$ into Eq. (2) leads to

$$\mathbf{S}(t) = \frac{-i\epsilon_0}{8}\left(\sum_{n=1}^{N}\sum_{m=1}^{N}\frac{1}{\omega_m}\mathbf{E}_n \times \mathbf{E}_m e^{-i(\omega_n+\omega_m)t}\right.$$
$$\left. + \sum_{n=1}^{N}\sum_{m=1}^{N}\frac{1}{\omega_m}\mathbf{E}_n^* \times \mathbf{E}_m e^{i(\omega_n-\omega_m)t} - \text{c.c.}\right), \tag{3}$$

where the asterisk and c.c. denote the complex conjugate. The time-averaged SAM density vector is given by

$$\mathbf{S} = \langle \mathbf{S}(t)\rangle = \lim_{T\to\infty}\frac{1}{T}\int_{-T/2}^{T/2}\mathbf{S}(t)dt. \tag{4}$$

Next we apply the relation

$$\lim_{T\to\infty}\frac{1}{T}\int_{-T/2}^{T/2}e^{\pm i(\omega_n-\omega_m)t}dt = \delta_{nm}, \tag{5}$$

where δ_{nm} is the Kronecker delta and we note that the sum frequency terms in Eq. (3) vanish on averaging. It then follows that

$$\mathbf{S} = \sum_{n=1}^{N}\mathbf{S}_n, \tag{6}$$

where

$$\mathbf{S}_n = \frac{\epsilon_0}{4\omega_n}\text{Im}(\mathbf{E}_n^* \times \mathbf{E}_n) \tag{7}$$

is the SAM density vector of the monochromatic field component at angular frequency ω_n [4,5], with Im denoting the imaginary part.

The spin vector of the total electric field is [12,19]

$$\mathbf{n} = \text{Im}\langle \boldsymbol{\mathcal{E}}^*(t) \times \boldsymbol{\mathcal{E}}(t)\rangle. \tag{8}$$

Performing the averaging as above results in

$$\mathbf{n} = \sum_{n=1}^{N}\mathbf{n}_n, \tag{9}$$

where

$$\mathbf{n}_n = \text{Im}(\mathbf{E}_n^* \times \mathbf{E}_n) \tag{10}$$

is the spin vector related to a single frequency component of the field.

Physically, the SAM density vector $\mathbf{S}$ describes the spin angular momentum per unit volume at a point, while $\mathbf{n}$ is closely linked to the polarization state and can be viewed as expressing the direction around which the electric vector circulates [11]. For a monochromatic field these vectors are parallel, as seen explicitly from Eqs. (7) and (10). The electric field of monochromatic light draws in general an ellipse in

a plane orthogonal to $\mathbf{n}$ and the orientation of this plane may be different at different points. Further, the magnitude of $\mathbf{n}$ is directly given by the helicity of the field [12]. These properties are restricted to monochromatic light, which is an idealized concept even though in many situations it provides a sufficiently accurate description of the field.

In practice, however, both synthetic and natural optical fields are polychromatic, for which the electric vector is not necessarily restricted to a plane and the average intensity in all three orthogonal directions may be nonzero for any orientation of the reference frame. It is evident from Eqs. (6), (7), (9), and (10) that in such a case $\mathbf{S}$ and $\mathbf{n}$ are not necessarily parallel due to the frequency factor $1/\omega_n$. In other words, for polychromatic 3D light the SAM density vector is not generally aligned to the direction $\mathbf{n}$ around which the electric field, on average, whirls. We also note that in this case the spin vector $\mathbf{n}$ is proportional to the helicity-weighted average of the corresponding (unit) direction vectors of the monochromatic components. This is clear from Eq. (9) by writing $\mathbf{n}_n = s_{3,n}\hat{\mathbf{u}}_n$ [12], where $s_{3,n}$ is the helicity related to $\mathbf{E}_n$ and $\hat{\mathbf{u}}_n$ is the unit vector normal to the polarization plane of $\mathbf{E}_n$.

B. Polarization properties

The subsequent discussion of the properties of optical spin in tight focusing requires the introduction of some polarimetric notions of the incident beam and of the focal field. The beam is a two-component field which can be expressed as $\mathbf{E}(t) = [E_x(t), E_y(t)]^\text{T}$, where T denotes the transpose, while the focal field necessitates a three-component representation $\mathbf{E}(t) = [E_x(t), E_y(t), E_z(t)]^\text{T}$. The structure of Eq. (1) holds for both types of fields, but for the former the vector amplitudes $\mathbf{E}_n$ are composed of two components only. The time-averaged polarization matrix representing the polarization properties at a point is given by [10,20]

$$\boldsymbol{\Phi} = \langle \boldsymbol{\mathcal{E}}^*(t)\boldsymbol{\mathcal{E}}^\text{T}(t)\rangle = \sum_{n=1}^{N}\mathbf{E}_n^*\mathbf{E}_n^\text{T}. \tag{11}$$

The matrix $\boldsymbol{\Phi}$ is evidently a sum of the polarization matrices related to the individual monochromatic field components. In addition, for a two-component (three-component) field the polarization matrix is a 2×2 (3×3) matrix. In both cases the intensity of the field is $I = \text{tr}\boldsymbol{\Phi}$, where tr stands for the trace.

The degree of polarization associated with the incident beam is given by

$$P = \left(1 - \frac{4\det\boldsymbol{\Phi}}{\text{tr}^2\boldsymbol{\Phi}}\right)^{1/2}, \tag{12}$$

where det denotes the determinant. The value of P is between zero and one, reflecting a fully unpolarized and a fully polarized beam, respectively. The dimensionality of the focal (three-component) field is characterized by the polarimetric dimension [21]

$$D = 3 - 2d, \tag{13}$$

where

$$d = \left[\frac{3}{2}\left(\frac{\text{tr}(\text{Re}^2\boldsymbol{\Phi})}{\text{tr}^2(\text{Re}\boldsymbol{\Phi})} - \frac{1}{3}\right)\right]^{1/2}. \tag{14}$$

The quantity d describes the intensity anisotropy of the polarization state [22] and is bounded as $0 \leqslant d \leqslant 1$. The polarimetric dimension therefore obeys $1 \leqslant D \leqslant 3$, with the lower and upper limits corresponding to one-dimensional light of maximal intensity anisotropy and intensity-isotropic 3D light, respectively. The value $D > 2$ is a clear signature of a genuine 3D field character. However, for $D \leqslant 2$ the intensity in all three orthogonal directions may still be nonzero for all orientations of the frame, i.e., the field is a true 3D field.

III. LISSAJOUS BEAMS

In this work we consider bichromatic Lissajous beams composed of two monochromatic fields with different frequencies and polarization states [23–26]. The complex electric field of such a superposition is of the form of Eq. (1) with $N = 2$, and

$$\mathbf{E}_n = a_n e^{i\phi_n} \hat{\mathbf{e}}_n, \quad n \in (1, 2), \tag{15}$$

where a_n, ϕ_n, and $\hat{\mathbf{e}}_n$ are the real amplitude, phase, and (complex) polarization unit vector for the nth wave, respectively. In Cartesian coordinates, the polarization vectors are expressed as

$$\hat{\mathbf{e}}_n = \alpha_n \hat{\mathbf{e}}_x + \beta_n \hat{\mathbf{e}}_y, \quad n \in (1, 2), \tag{16}$$

where α_n and β_n are complex coefficients, with $|\alpha_n|^2 + |\beta_n|^2 = 1$, and $\hat{\mathbf{e}}_x$ and $\hat{\mathbf{e}}_y$ are the unit (column) vectors in the x and y directions. The polarization curve, i.e., the trajectory of the tip of electric field vector $\mathbf{E}(t)$, is governed by the parameters a_n, ϕ_n, $\hat{\mathbf{e}}_n$, and ω_n, $n \in (1, 2)$.

The total (time-averaged) spin vector is obtained from Eqs. (9) and (10) as $\mathbf{n} = \mathbf{n}_1 + \mathbf{n}_2$, with

$$\mathbf{n}_n = i a_n^2 (\alpha_n \beta_n^* - \alpha_n^* \beta_n) \hat{\mathbf{e}}_z, \quad n \in (1, 2). \tag{17}$$

In addition, according to Eqs. (6) and (7), the total SAM vector is given by

$$\mathbf{S} = \frac{\epsilon_0}{4} \left(\frac{1}{\omega_1} \mathbf{n}_1 + \frac{1}{\omega_2} \mathbf{n}_2 \right). \tag{18}$$

Employing Eq. (11), the polarization matrix of the beam is found to be

$$\boldsymbol{\Phi} = \begin{pmatrix} a_1^2 |\alpha_1|^2 + a_2^2 |\alpha_2|^2 & a_1^2 \alpha_1^* \beta_1 + a_2^2 \alpha_2^* \beta_2 \\ a_1^2 \alpha_1 \beta_1^* + a_2^2 \alpha_2 \beta_2^* & a_1^2 |\beta_1|^2 + a_2^2 |\beta_2|^2 \end{pmatrix}, \tag{19}$$

and the degree of polarization P can be calculated from Eq. (12).

Next we introduce two Lissajous beams whose SAM density vector and spin vector in the focal region are studied in the next section. In the first case, the polarization states are right-hand and left-hand circular polarization states with $\hat{\mathbf{e}}_1 = (\hat{\mathbf{e}}_x + i\hat{\mathbf{e}}_y)/\sqrt{2}$ and $\hat{\mathbf{e}}_2 = (\hat{\mathbf{e}}_x - i\hat{\mathbf{e}}_y)/\sqrt{2}$, respectively. The degree of polarization equals $P = |a_1^2 - a_2^2|/(a_1^2 + a_2^2)$, while the spin vectors of the constituent beams are $\mathbf{n}_1 = a_1^2 \hat{\mathbf{e}}_z$ and $\mathbf{n}_2 = -a_2^2 \hat{\mathbf{e}}_z$, where $\hat{\mathbf{e}}_z$ is the unit vector in the z direction. We note that when $a_1 = a_2$, the field is unpolarized ($P = 0$) and carries no spin vector, i.e., $\mathbf{n} = \mathbf{0}$, but the SAM density vector is nonzero, $\mathbf{S} = (\epsilon_0 I/8)(1/\omega_1 - 1/\omega_2)\hat{\mathbf{e}}_z$. The situation is opposite when $\omega_2 a_1^2 = \omega_1 a_2^2$ holds, i.e., the SAM density vector is zero $\mathbf{S} = \mathbf{0}$, while the spin vector is nonzero
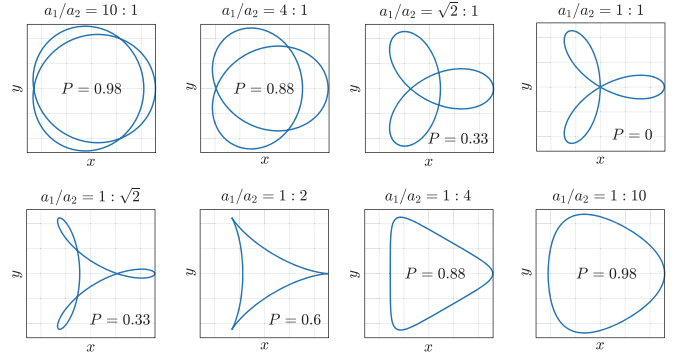

FIG. 1. Polarization curves for the bichromatic Lissajous beams having $\hat{\mathbf{e}}_1 = (\hat{\mathbf{e}}_x + i\hat{\mathbf{e}}_y)/\sqrt{2}$, $\hat{\mathbf{e}}_2 = (\hat{\mathbf{e}}_x - i\hat{\mathbf{e}}_y)/\sqrt{2}$, $\omega_1 = 2\omega_2$, and $\phi_1 = \phi_2 = 0$, for various ratios a_1/a_2. The values for the degree of polarization P are also shown.

$\mathbf{n} = (a_1^2 - a_2^2)\hat{\mathbf{e}}_z$. The degree of polarization now takes the form $P = |\omega_1 - \omega_2|/(\omega_1 + \omega_2)$.

In Fig. 1 we show the polarization curves of the above Lissajous beam for various amplitude ratios a_1/a_2. In the illustrations we set $\omega_1 = 2\omega_2$ and $\phi_1 = \phi_2 = 0$ and display also the values for the degree of polarization. We find that the (real-value) electric field $\mathbf{E}(t)$ traces out symmetric closed curves with three, one, or zero self-intersections. For $a_1/a_2 \gg 1$, the polarization curve approaches that corresponding to the polarization state $\hat{\mathbf{e}}_1$ (circle), while for $a_1/a_2 \ll 1$ it reduces to that of $\hat{\mathbf{e}}_2$ (also circle). In both limiting cases, the degree of polarization approaches unity. For $a_1/a_2 = 1$, the field is unpolarized and its polarization curve shows a Lissajous-like curve with only one self-intersection.

In the second case, we set the polarization states as $\hat{\mathbf{e}}_1 = \hat{\mathbf{e}}_x$ and $\hat{\mathbf{e}}_2 = \hat{\mathbf{e}}_y$, corresponding to orthogonal linear polarizations. The degree of polarization has the same expression as in the first case. However, the spin vectors vanish $\mathbf{n}_1 = \mathbf{n}_2 = \mathbf{0}$. Therefore, the field carries neither a spin vector nor a SAM density vector. The polarization curves of such a field with different ratios a_1/a_2 are presented in Fig. 2 and we find that the electric field $\mathbf{E}(t)$ traces out a curved line. In the limiting case when $a_1/a_2 \gg 1$, the polarization curve tends to a straight line in the x direction (x-polarized beam), while when
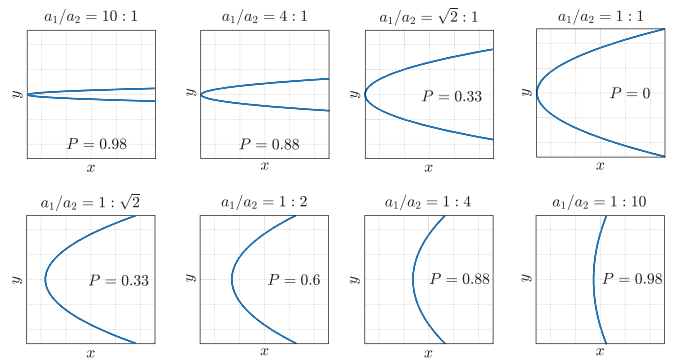

FIG. 2. Polarization curves for the bichromatic optical Lissajous fields with $\hat{\mathbf{e}}_1 = \hat{\mathbf{e}}_x$, $\hat{\mathbf{e}}_2 = \hat{\mathbf{e}}_y$, $\omega_1 = 2\omega_2$, and $\phi_1 = \phi_2 = 0$. The varied ratio a_1/a_2 and the related degree of polarization are shown in each panel.

$a_1/a_2 \ll 1$ it approaches a line in the y direction (y-polarized beam).

IV. TIGHTLY FOCUSED LISSAJOUS BEAMS

In this section we study the spin properties of tightly focused bichromatic Lissajous beams. The focusing system is an aplanatic objective lens with high numerical aperture and its operation is treated within the Richards-Wolf formalism [27]. A description of the formalism can be found in many works [17,28,29] and is not presented here. The electric field in the focal region is expressible as

$$\mathcal{E}^{(f)}(\mathbf{r}, t) = \mathbf{E}_1^{(f)}(\mathbf{r})e^{-i\omega_1 t} + \mathbf{E}_2^{(f)}(\mathbf{r})e^{-i\omega_2 t}, \quad (20)$$

where we have introduced a position vector $\mathbf{r} = (x, y, z)$ and the superscript f indicates a focal field. Further, $\mathbf{E}_1^{(f)}(\mathbf{r})$ and $\mathbf{E}_2^{(f)}(\mathbf{r})$ are the three-component electric vectors produced by the incident two-component vectors $\mathbf{E}_1$ and $\mathbf{E}_2$, respectively, given in Eq. (15). The vectors $\mathbf{E}_1^{(f)}(\mathbf{r})$ and $\mathbf{E}_2^{(f)}(\mathbf{r})$ result from the Richards-Wolf vectorial diffraction integral and the spin characteristics of $\mathcal{E}^{(f)}(\mathbf{r}, t)$ are obtained with the formalism developed in Sec. II. In the two situations considered below, we take the numerical aperture to be equal to 0.95, while the focal length of the lens is $f = 3$ mm. In addition, the focusing system is placed in a vacuum environment and the wavelengths for the incident constituent fields that form the Lissajous beams are $\lambda_1 = 300$ nm and $\lambda_2 = 600$ nm, i.e., the angular frequencies obey $\omega_1 = 2\omega_2$.

A. Superposition of circularly polarized beams

Next we assess the spin properties of the field obtained by focusing a bichromatic Lissajous beam with $\hat{\mathbf{e}}_1 = (\hat{\mathbf{e}}_x + i\hat{\mathbf{e}}_y)/\sqrt{2}$, $\hat{\mathbf{e}}_2 = (\hat{\mathbf{e}}_x - i\hat{\mathbf{e}}_y)/\sqrt{2}$, and $a_1 = a_2 = 1$. Such an incident beam is unpolarized $P = 0$ and the spin vector vanishes $\mathbf{n} = \mathbf{0}$, while the SAM density vector $\mathbf{S}$ is nonzero. Figures 3(a) and 3(b) show the focal-plane spatial distributions for the components of the spin vector and SAM density vector, respectively. In addition, Fig. 3(c) depicts the entire vectors $\mathbf{n}$ and $\mathbf{S}$, whereas Fig. 3(d) illustrates the angular difference of their directions. Unlike the incident beam, the focal field carries a nonzero spin vector in addition to the SAM density vector. The transverse spin $\mathbf{n}_\perp = (n_x, n_y)$ originates from the generation of the out-of-phase longitudinal field component. Instead, the longitudinal spin n_z is due to the different focusing properties of the waves with different wavelengths. More precisely, the input wave with smaller wavelength λ_1 will create a tighter focal spot with larger intensity (when $a_1 = a_2$) than the other wave. Consequently, the spatial distribution of $n_{z1}(\mathbf{r})$ is tighter than that of $n_{z2}(\mathbf{r})$ and the total longitudinal spin obeys $n_z(\mathbf{r}) = n_{z1}(\mathbf{r}) + n_{z2}(\mathbf{r}) \neq 0$. From the spatial distributions of the spin vector and the SAM density vector in Fig. 3(c), we observe a notable angular difference between the two vectors within the region of significant spin values. It is seen from Fig. 3(d) that the angular separation can be more than 30°. The directional difference is explained as follows. Figure 3(c) indicates that the transverse vectors $\mathbf{n}_\perp$ and $\mathbf{S}_\perp = (S_x, S_y)$ show the vortex distributions of the same shape. However, the ratios of the transverse and longitudinal components in $\mathbf{n}$ and $\mathbf{S}$ are different, which causes the angular difference.
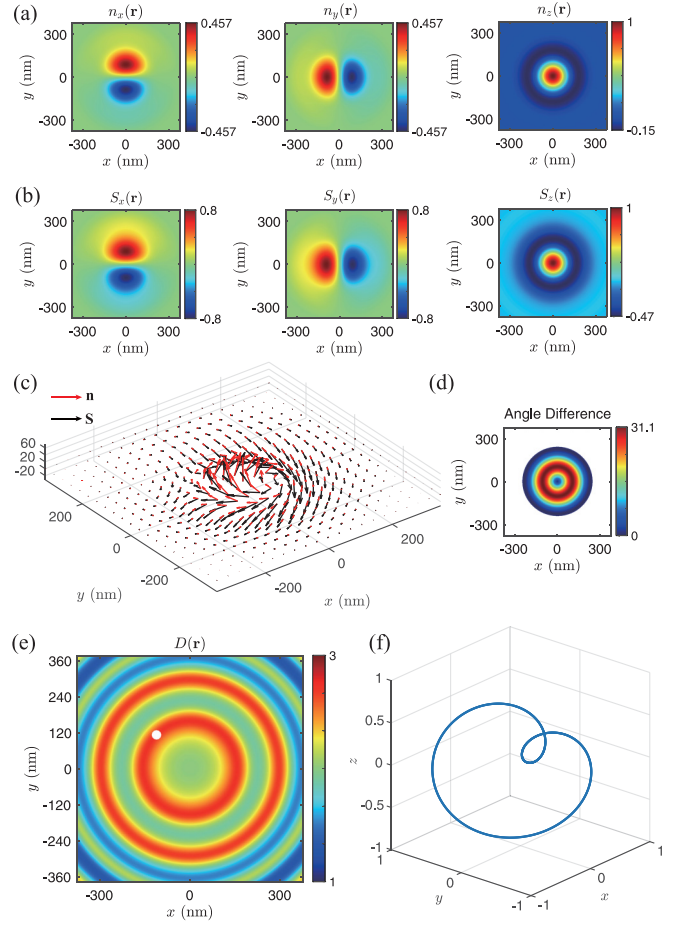

FIG. 3. Focal-plane spatial distributions of (a) the components of the spin vector $\mathbf{n} = (n_x, n_y, n_z)$; (b) the components of the SAM density vector $\mathbf{S} = (S_x, S_y, S_z)$; (c) the spin vector (red) and the SAM density vector (black), with the vertical axis showing the strengths of the z components in arbitrary units; (d) the angular separation of $\mathbf{n}$ and $\mathbf{S}$ in the region where $|\mathbf{n}|$ and $|\mathbf{S}|$ are larger than 10% of their maximum values; (e) the polarimetric dimension D; and (f) the electric-field trajectory at a point where D reaches its maximum value [white dot in (e)]. The parameters of the incident Lissajous beam are $\lambda_1 = 300$ nm, $\lambda_2 = 600$ nm, $a_1 = a_2 = 1$, $\phi_1 = \phi_2 = 0$, $\hat{\mathbf{e}}_1 = (\hat{\mathbf{e}}_x + i\hat{\mathbf{e}}_y)/\sqrt{2}$, and $\hat{\mathbf{e}}_2 = (\hat{\mathbf{e}}_x - i\hat{\mathbf{e}}_y)/\sqrt{2}$.

The angular separation of $\mathbf{n}$ and $\mathbf{S}$ needs to be contrasted with the dimensionality of the polarization state. Figure 3(e) shows the spatial distribution of the polarimetric dimension D of Eq. (13) in the focal plane. We find that D can assume values larger than 2, which is an exclusive indication of the genuine 3D polarization character of the field. In particular, compared to Fig. 3(d), we observe that large angular separations of $\mathbf{n}$ and $\mathbf{S}$ occur in regions where $D > 2$. This is as expected since the spin vector and SAM density vector point in the same or opposite directions for beamlike fields for which necessarily $D \leqslant 2$ [12]. In Fig. 3(f) we plot the polarization trajectory of the electric field $\mathbf{E}(t)$ in the focal plane at a spatial point [marked by a white dot in Fig. 3(e)] where D reaches its maximum value. We see that within one cycle all three electric-field components are strong, consistently with the 3D character.
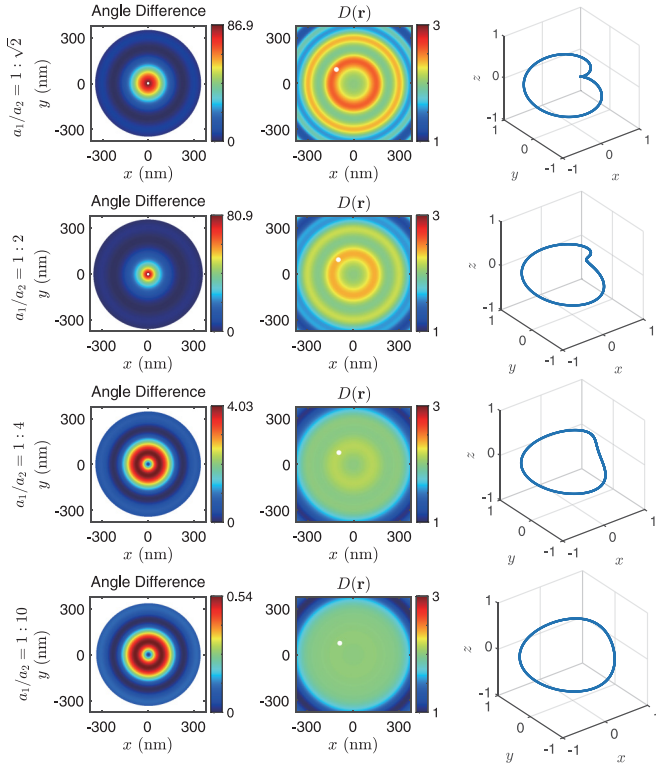
FIG. 4. Focal-plane spatial distributions of the angle between **n** and **S** in the region where $|\mathbf{n}|$ and $|\mathbf{S}|$ are larger than 10% of their maximum values (left column), the polarimetric dimension D (middle column), and the electric-field trajectory at a spatial point (white dot in D plots) where D reaches its maximum value (right column). The rows correspond to different a_1/a_2 values marked next to them. The parameters of the incident Lissajous beam are $\lambda_1 = 300$ nm, $\lambda_2 = 600$ nm, $a_1 = a_2 = 1$, $\phi_1 = \phi_2 = 0$, $\hat{\mathbf{e}}_1 = (\hat{\mathbf{e}}_x + i\hat{\mathbf{e}}_y)/\sqrt{2}$, and $\hat{\mathbf{e}}_2 = (\hat{\mathbf{e}}_x - i\hat{\mathbf{e}}_y)/\sqrt{2}$.
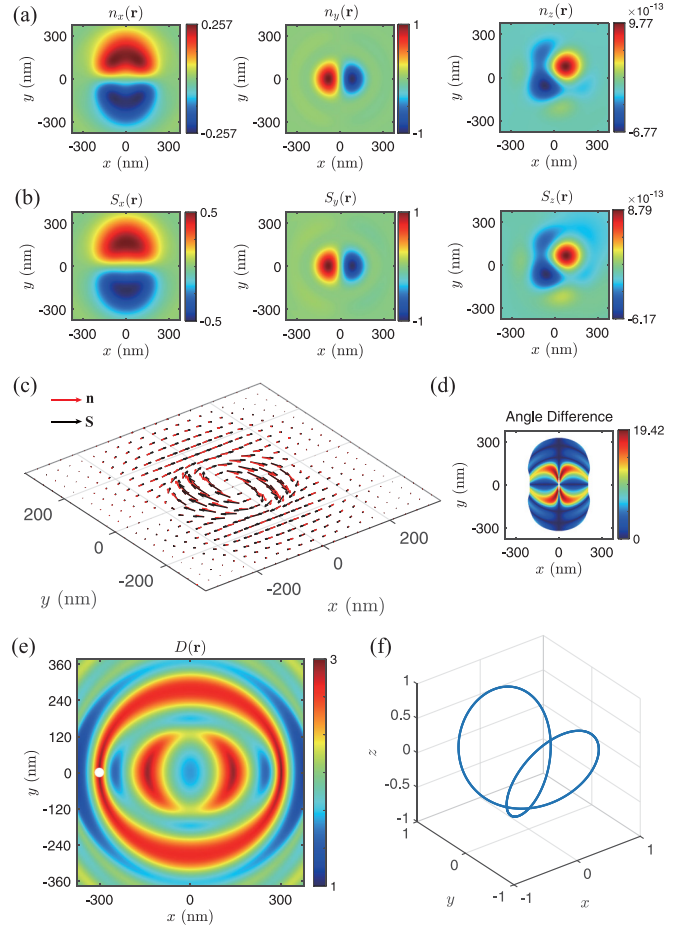

FIG. 5. Same as Fig. 3 except the Jones vectors related to the incident Lissajous beam are $\hat{\mathbf{e}}_1 = \hat{\mathbf{e}}_x$ and $\hat{\mathbf{e}}_2 = \hat{\mathbf{e}}_y$, corresponding to orthogonal linear polarizations.

Figure 4 shows, for various a_1/a_2 values, the focal-plane spatial distributions of the angle between **n** and **S**, the polarimetric dimension D, and the polarization curve at a spatial point where D reaches its maximum value. It is found that for $a_1/a_2 = 1/\sqrt{2}$ the angular separation of **n** and **S** can reach a value close to $90°$, i.e., the two spin vectors displaying different physical information can be almost orthogonal. Decreasing the ratio, the angle decreases and with small a_1/a_2 values the spin vector and SAM density vector are practically parallel and the field is essentially a 2D field. In the limiting case of $a_1/a_2 \ll 1$, the focal-plane polarization properties coincide with those of a focused plane wave having wavelength λ_2 and polarization state $\hat{\mathbf{e}}_2$.

B. Superposition of linearly polarized beams

We now consider tight focusing of a bichromatic Lissajous beam with $\hat{\mathbf{e}}_1 = \hat{\mathbf{e}}_x$, $\hat{\mathbf{e}}_2 = \hat{\mathbf{e}}_y$, and $a_1 = a_2 = 1$. Figures 5(a)–5(d) show the focal-plane spatial distributions of the spin vector and SAM density vector (components and full vectors) as well as the angle difference between the two vectors. We find that both **n** and **S** are purely transverse ($n_z = 0$). The origin of this feature is that the focal transverse field components are in phase when the incident beam is linearly polarized.

We also note that n_x and S_x are contributed mainly by the incident y-polarized component, while the x-polarized wave contributes effectively to n_y and S_y. Since the wavelength for the x-polarized beam is smaller than that for the y-polarized wave, the spatial distributions of n_y and S_y are tighter than those of n_x and S_x. As a result, the spin vector and SAM density vector in Fig. 5(c) show asymmetric azimuthal vortex distributions. The maximal angle difference of **n** and **S** is found to be about $19.5°$.

Figure 5(e) shows the spatial distribution of the polarimetric dimension D in the focal plane. Similarly to the case in Sec. IV A, D can assume values larger than 2, indicating a true 3D polarization character of the focal field. The evolution curve of $\mathbf{E}(t)$ in Fig. 5(f) corresponds to a spatial point where D reaches its maximum value [white dot in Fig. 5(e)] and likewise reflects the 3D character of the field since all three orthogonal components are strong.

Figure 6 shows the focal-plane spatial distributions of the angular difference of **n** and **S**, the polarimetric dimension D, and the polarization curve in a spatial point where D reaches its maximum value for various a_1/a_2 ratios. We find that when a_1/a_2 decreases, the angle difference in general decreases within the region of effective spin and the field approaches a 2D field. Compared to the case in Sec. IV A where the
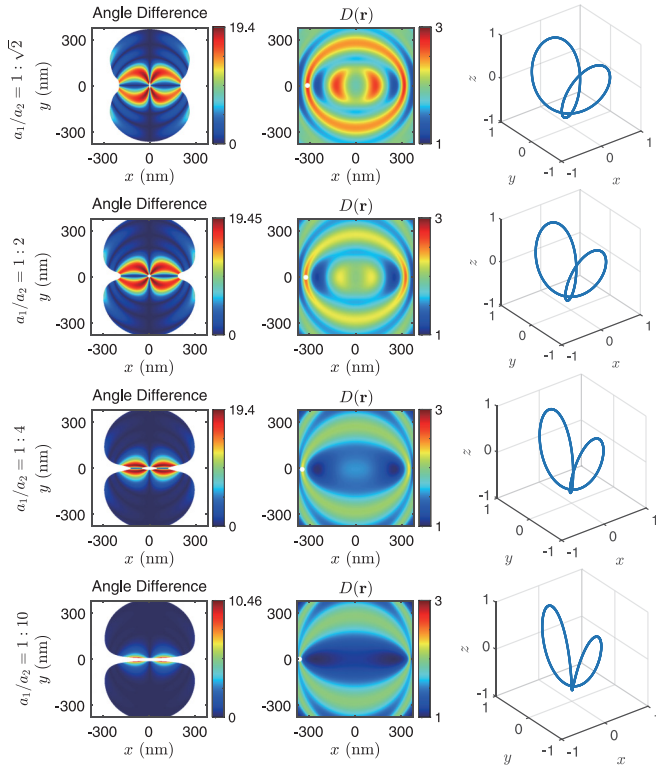
FIG. 6. Same as Fig. 4 except the Jones vectors related to the incident Lissajous beam are $\hat{\mathbf{e}}_1 = \hat{\mathbf{e}}_x$ and $\hat{\mathbf{e}}_2 = \hat{\mathbf{e}}_y$, corresponding to orthogonal linear polarizations.

Lissajous beam consists of circularly polarized monochromatic waves, the angular deviations of **n** and **S** are much smaller.

V. CONCLUSION

We have analyzed the directional difference of the SAM density vector and the spin vector in 3D optical fields generated in tight focusing of bichromatic Lissajous beams. The former quantity has its origin in electrodynamics, whereas the latter is linked to the polarization properties of the field and can be viewed as specifying an average direction around which the electric vector circulates. For monochromatic light the SAM density vector and spin vector are parallel and for polychromatic 2D fields they can be also antiparallel [12]. Other situations are encountered only in the case of genuine 3D fields, which are necessarily polychromatic and have nonzero intensity in all directions. In such fields the spin vectors of different frequencies, expressing the spectral polarization characteristic, can point in different directions. The total spin vector is the helicity-weighted sum of the constituent (unit) direction vectors, while the SAM density vector includes an additional frequency-dependent weighting, resulting in the different directions for the two vectors. In this work we demonstrated a case where the angular separation of the vectors is almost 90°, i.e., the SAM density and spin vectors are nearly orthogonal. Consequently, information on the spin properties of light that the two vectors provide may be different. This notion is particularly important in the context of 3D light fields.

[1] S. M. Barnett, Rotation of electromagnetic fields and the nature of optical angular momentum, J. Mod. Opt. **57**, 1339 (2010).

[2] M. Mansuripur, Spin and orbital angular momenta of electromagnetic waves in free space, Phys. Rev. A **84**, 033838 (2011).

[3] K. Y. Bliokh, J. Dressel, and F. Nori, Conservation of spin and orbital angular momenta in electromagnetism, New J. Phys. **16**, 093037 (2014).

[4] K. Y. Bliokh and F. Nori, Transverse and longitudinal angular momenta of light, Phys. Rep. **592**, 1 (2015).

[5] A. Aiello, P. Banzer, M. Neugebauer, and G. Leuch, From transverse angular momentum to photonic wheels, Nat. Photonics **9**, 789 (2015).

[6] S. M. Barnett, L. Allen, R. P. Cameron, C. R. Gilson, M. J. Padgett, F. C. Speirits, and A. M. Yao, On the natures of the spin and orbital parts of optical angular momentum, J. Opt. **18**, 064004 (2016).

[7] A. I. Arbab, New derivation of the spin of the electromagnetic field, Optik **184**, 436 (2019).

[8] A. Aiello, Helicity, chirality, and spin of optical fields without vector potentials, Phys. Rev. A **106**, 043519 (2022).

[9] C. Brosseau, *Fundamentals of Polarized Light: A Statistical Optics Approach* (Wiley, New York, 1998).

[10] J. J. Gil and R. Ossikovski, *Polarized Light and the Mueller Matrix Approach*, 2nd ed. (CRC, Boca Raton, 2022).

[11] M. A. Alonso, Geometric descriptions for the polarization of nonparaxial light: a tutorial, Adv. Opt. Photonics **15**, 176 (2023).

[12] J. J. Gil, A. Norrman, A. T. Friberg, and T. Setälä, Spin of random stationary light, Phys. Rev. A **107**, 053518 (2023).

[13] K. Y. Bliokh, A. Y. Bekshaev, and F. Nori, Extraordinary momentum and spin in evanescent waves, Nat. Commun. **5**, 3300 (2014).

[14] M. Neugebauer, T. Bauer, A. Aiello, and P. Banzer, Measuring the transverse spin density of light, Phys. Rev. Lett. **114**, 063901 (2015).

[15] M. Neugebauer, J. S. Eismann, T. Bauer, and P. Banzer, Magnetic and electric transverse spin density of spatially confined light, Phys. Rev. X **8**, 021042 (2018).

[16] J. S. Eismann, P. Banzer, and M. Neugebauer, Spin-orbit coupling affecting the evolution of transverse spin, Phys. Rev. Res. **1**, 033143 (2019).

[17] L. Novotny and B. Hecht, *Principles of Nano-Optics*, 2nd ed. (Cambridge University Press, Cambridge, 2012).

[18] Y. Chen, A. Norrman, S. A. Ponomarenko, and A. T. Friberg, Optical coherence and electromagnetic surface waves, Prog. Opt. **65**, 105 (2020).

[19] J. J. Gil, A. T. Friberg, A. Norrman, and T. Setälä, Effect of polarimetric nonregularity on the spin of three-dimensional polarization states, New J. Phys. **23**, 063059 (2021).

[20] L. Mandel and E. Wolf, *Optical Coherence and Quantum Optics* (Cambridge University Press, Cambridge, 1995).

[21] A. Norrman, A. T. Friberg, J. J. Gil, and T. Setälä, Dimensionality of random light fields, J. Eur. Opt. Soc.-Rapid Publ. **13**, 36 (2017).

[22] J. J. Gil, A. Norrman, A. T. Friberg, and T. Setälä, Intensity and spin anisotropy of three-dimensional polarization states, Opt. Lett. **44**, 3578 (2019).

[23] I. Freund, Bichromatic optical Lissajous fields, Opt. Commun. **226**, 351 (2003).

[24] D. A. Kessler and I. Freund, Lissajous singularities, Opt. Lett. **28**, 111 (2003).

[25] A. Fleischer, O. Kfir, T. Diskin, P. Sidorenko, and O. Cohen, Spin angular momentum and tunable polarization in high-harmonic generation, Nat. Photonics **8**, 543 (2014).

[26] E. Pisanty, G. J. Machado, V. Vicuña-Hernández, A. Picón, A. Celi, J. P. Torres, and M. Lewenstein, Knotting fractional-order knots with the polarization state of light, Nat. Photonics **13**, 569 (2019).

[27] B. Richards and E. Wolf, Electromagnetic diffraction in optical system, II. Structure of the image field in an aplanatic system, Proc. R. Soc. London Ser. A **253**, 358 (1959).

[28] R. Tong, Z. Dong, Y. Chen, F. Wang, Y. Cai, and T. Setälä, Fast calculation of tightly focused random electromagnetic beams: controlling the focal field by spatial coherence, Opt. Express **28**, 9713 (2020).

[29] Y. Chen, F. Wang, Z. Dong, Y. Cai, A. Norrman, J. J. Gil, A. T. Friberg, and T. Setälä, Structure of transverse spin in focused random light, Phys. Rev. A **104**, 013516 (2021).